Research Article

Tamal Das, Manvinder Kaur*, Navneet Kaur, Pradip K. Bhowmik, Haesook Han, Harvinder Singh Sohal*, and Fohad Mabood Husain

Greener and magnetic Fe₃O₄ nanoparticles as a recyclable catalyst for Knoevenagel condensation and degradation of industrial Congo red dye

https://doi.org/10.1515/gps-2024-0257 received December 17, 2024; accepted March 29, 2025

Abstract: This study investigates the environmentally friendly synthesis of Fe₃O₄ nanoparticles using basil leaf extract as a sustainable precursor. The resulting basil-Fe₃O₄ nanoparticles were extensively characterized through Fourier-Transform infrared, UV-Vis, scanning electron microscopy, energy-dispersive spectroscopy, X-ray diffraction, and VSM to verify their structural, morphological, and magnetic properties. Optical analysis showed a prominent absorption peak at 263 nm and a band gap energy of 3.87 eV, suggesting its potential for photocatalytic applications. The catalytic performance of basil-Fe₃O₄ was tested in the synthesis of 2-benzylidene malononitrile derivatives under microwave irradiation, achieving up to 98% purity in crystalline form across 12 examples involving aromatic and heteroaromatic aldehydes with malononitrile. The catalyst exhibited excellent reusability with minimal loss of activity over several cycles, highlighting its potential for greener and more sustainable chemical processes. Additionally, the photocatalytic performance of basil–Fe₃O₄ was evaluated for the degradation of Congo red dye, achieving an impressive 97% degradation efficiency under UV irradiation. Kinetic analysis indicated a high regression coefficient and a significant reaction rate constant, confirming its superior activity. The limit of detection and limit of quantification were determined to be 32.8 and 99.16 mg·L⁻¹, respectively, affirming the method's sensitivity and reliability for detecting Congo red dye. Remarkably, even a small amount (5%) of the catalyst enabled efficient degradation under low UV exposure, showcasing its potential for large-scale wastewater treatment. The dual functionality of basil–Fe₃O₄ nanoparticles in both organic synthesis and environmental remediation highlights its promise for sustainable advancements in green chemistry and wastewater treatment applications.

Keywords: green chemistry, recyclable magnetic nanoparticles, Knoevenagel condensation, heterogeneous catalyst, dye degradation

1 Introduction

Nanocatalysis is one of the thrust areas for synthetic organic chemists to produce compounds in small time and with high selectivity [1]. The yield of the reaction increases to a greater extent because it decreases the energy barrier between reactants and products [2]. To support green innovation, it may also reduce waste based on reagents and enhance reaction selectivity at a strategic distance from the unwanted by-product [3]. One of the finest ideas for green science is to design the ideal nanocatalyst for the selected synthetic challenge [4]. Typically nanoparticles of Ag [5], Zn [6], Ni [7], Cu [8, 9], Co [10], and Mn [6] supported on cellulose [11], silica [12], charcoal [13], alumina [14], chitosan [15], and β-cyclodextrins [16] were designed for one-time usage because during the separation process, researchers lost the catalyst because they are focused on their final product, whereas the magnetic catalytic nanocomposite can be employed repeatedly within a single reaction as it can be separated easily [17]. Magnetic

Tamal Das, Navneet Kaur: Department of Chemistry, Materials and Natural Product Laboratory, Chandigarh University, Gharuan-140 413, Mohali, Punjab, India

Pradip K. Bhowmik, Haesook Han: Department of Chemistry and Biochemistry, University of Nevada Las Vegas, 4505 S. Maryland Parkway, Box 454003, Las Vegas, NV, 89154, United States of America **Fohad Mabood Husain:** Department of Food Science and Nutrition, College of Food and Agriculture Sciences, King Saud University, Riyadh, 11451, Saudi Arabia

^{*} Corresponding author: Manvinder Kaur, Department of Chemistry, Materials and Natural Product Laboratory, Chandigarh University, Gharuan-140 413, Mohali, Punjab, India; Chitkara University Institute of Engineering and Technology, Chitkara University, Rajpura-140 401, Punjab, India, e-mail: manvinder.2k50@gmail.com

^{*} Corresponding author: Harvinder Singh Sohal, Department of Chemistry, Materials and Natural Product Laboratory, Chandigarh University, Gharuan-140 413, Mohali, Punjab, India, e-mail: drharvinder.cu@gmail.com

nanocomposites demonstrate distinct nanoscale characteristics and have garnered significant interest in various magnetic systems [18,19]. Fe₃O₄, the most stable form of iron oxide, is an eco-friendly semiconductor characterized by a band gap energy of 2.1 eV [20]. Metal oxide nanoparticles possess impressive optical characteristics, such as adjustable band gaps and excellent photocatalytic efficiency, which makes them ideal for environmental applications. Their capacity to alter electronic structures significantly improves photocatalytic degradation, an essential process for wastewater treatment [21].

From the literature, several reports indicate that Knoevenagel condensation, between aldehydes or ketones and active methylene compounds in the presence of the base, is one of the key steps to producing many bioactive α,β-unsaturated carbonyl or nitrile compounds, which are important intermediates in the synthesis of heterocycles, natural products, and various medicinally significant compounds, including anticancer, antimicrobial, and antiinflammatory agents [22,23]. Since this step is time-consuming and is responsible for low yields of final organic compounds, researchers applied variant methodologies to overcome this problem. However, existing methodologies have advantages over others, but they also have many disadvantages in terms of expensive catalysts, expensive purification techniques, and low purity of final products [24]. Therefore, the growth of a clean and effective procedure for the synthesis of benzylidene malononitrile derivatives is still timely [25]. A variety of catalytic systems have been investigated for Knoevenagel condensation, such as homogeneous catalysts (amines, organobases) and heterogeneous catalysts (metal oxides, zeolites, and nanocatalysts). While homogeneous catalysts are known for their high selectivity, they face challenges with recovery [24]. On the contrary, heterogeneous catalysts offer advantages in terms of recyclability and stability. Recently, magnetic nanocatalysts have become increasingly popular because of their easy separation, larger surface area, and potential to facilitate greener and more efficient organic transformations [4].

Fe₃O₄ nanoparticles have been investigated as heterogeneous catalysts because of their magnetic properties, which facilitate easy separation and reuse [23]. A recent study showcased the use of Fe₃O₄ nanoparticles supported on microcrystalline cellulose as a heterogeneous catalyst for the sustainable multicomponent synthesis of 2,3'-biindoles, highlighting improved performance and reusability [26]. In recent years, using plant extracts for the green synthesis of nanoparticles has gained considerable attention because of their eco-friendly and sustainable characteristics [27]. Basil (*Ocimum basilicum*), a commonly found

herb, has been successfully used as a reducing and capping agent in the creation of iron oxide nanoparticles. The phytochemicals in basil help reduce metal ions and stabilize the resulting nanoparticles, providing a biocompatible alternative to traditional chemical synthesis methods. This method not only reduces environmental impact but also improves the functional properties of the nanoparticles, making them suitable for a range of catalytic and environmental applications [28].

The Fe₃O₄@HZSM-5 nano-magnetite catalyst was synthesized, showing strong magnetic properties and effective performance in removing metronidazole from contaminated samples. It achieved a high efficiency of 98% under optimal conditions and maintained good reusability, with 85% effectiveness after seven cycles, making it a promising candidate for environmental remediation [29]. Recent studies on CoFe₂O₄@methylcellulose (MC)/activated carbon nanohybrid adsorbents have demonstrated high efficiency in eliminating pharmaceutical pollutants, with metronidazole removal rates reaching up to 93% [30].

Congo red dye is a widely used synthetic azo dye in the textile, paper, and leather industries, but its presence in wastewater is a major environmental concern due to its toxicity, recalcitrance, and potential carcinogenicity [31]. Traditional methods of dye removal, such as chemical coagulation, adsorption, and membrane filtration, often fall short due to high operational costs, inefficiency, and the generation of secondary waste [32]. Consequently, the development of more sustainable and efficient approaches, such as photocatalytic degradation, has gained significant attention. Photocatalytic degradation offers a promising solution by utilizing catalysts, typically semiconductors, which can generate reactive oxygen species (ROS) under visible light or UV irradiation to break down dye molecules into non-toxic by-products [33].

Various catalysts, including metal oxides (such as ZnO, Fe₃O₄, and TiO₂), and composite materials have been explored for their ability to degrade Congo red dye effectively. Magnetic nanocomposites combine catalytic activity with the added advantage of easy recovery *via* magnetic separation, making them ideal for practical applications in wastewater treatment [31]. Magnetic Fe₃O₄ nanomaterials are gaining attention as effective options for removing emerging contaminants, such as synthetic dyes, due to their large surface area and simple separation process. For instance, a study introduced a Fe₃O₄-biochar composite catalyst that successfully degraded Fast Green dye, reaching approximately 89.3% degradation in just 60 min under optimal conditions [34].

In the present paper, we have described a Fe_3O_4 nanocatalyst derived from basil extract, which has dual applications in organic synthesis and wastewater treatment. It improves the Knoevenagel condensation process when subjected to

microwave irradiation, leading to higher yields and shorter reaction times. Furthermore, its excellent photocatalytic properties facilitate the effective degradation of Congo red dye. The catalyst is synthesized in an environmentally friendly manner, is recyclable, and can be magnetically recovered, making it a sustainable and economical option, aligning with the principles of green chemistry and sustainable development.

2 Experimental methods

2.1 Materials

The chemicals used in this study were obtained from Sigma Aldrich and utilized as received, without additional purification. Solvents were sourced from Changshu Song Sheng Fine Chemical. The basil leaves were gathered from the nearby region of Gharuan, Punjab, India, situated at 30.771545°N latitude and 76.5589309°E longitude.

2.2 Instruments

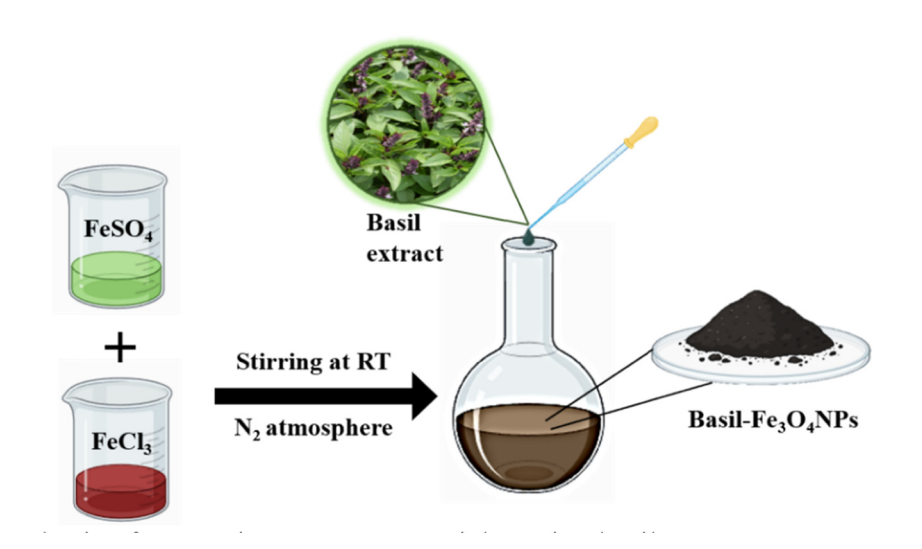
The melting points of the synthesized products were determined using a digital melting point apparatus and the open capillary method. The Fourier-transform infrared (FT-IR) spectra of the synthesized compounds were recorded in ATR mode using a Perkin Elmer Spectrum II instrument. ¹H NMR and ¹³C NMR spectra were acquired with a Bruker Avance NEO NMR spectrometer, using CDCl₃ as the solvent. The progress of reactions and purity of compounds were monitored via thin-layer chromatography (TLC) visualized under a UV chamber. Scanning electron microscopy (SEM) images of the Fe₃O₄ sample were obtained using a JSM IT500 microscope in high vacuum mode, with the imaging conditions ranging from 30 nm (30 kV) to 15 nm (1.0 kV). The elemental composition analysis of microscopic sections was conducted using energy-dispersive spectroscopy (EDS). X-ray diffraction (XRD) patterns of lyophilized samples were recorded using a Bruker D8 Advance instrument. The magnetic property of the nanocatalyst was studied with a Lake Shore 7410 Series vibrating sample magnetometer.

2.3 Preparation of basil leaf extract

The fresh basil leaves were harvested, thoroughly cleaned, and air-dried in the shade at room temperature for 6-7 days during the summer season. The dried leaves were ground into the fine powder. An ethanolic extract was prepared via maceration by combining 10 g of the powdered leaves with 100 mL of ethanol in a 250 mL beaker. followed by continuous stirring at room temperature for 24 h. The resulting extract was filtered and dried using a rotatory evaporator and then stored in an airtight vial at 4°C for future use.

2.4 Synthesis of magnetic basil-Fe₃O₄ nanoparticles

The basil-Fe₃O₄ nanoparticles, as shown in Scheme 1, were synthesized by the conventional chemical coprecipitation



Scheme 1: Synthesis of magnetic Fe₃O₄ nanoparticles using basil extract.

method, in which iron(II) sulfate solution and iron(III) chloride solution were added in a 2:1 molar ratio to a round-bottom flask and the solution was purged with nitrogen gas. After complete dissolution, 10 mL of ethanolic basil extract was slowly added to it dropwise and refluxed at 80°C for 2 h. The subsequent black precipitate was recovered through a magnet and washed successively with distilled water and acetone. The resultant product was dried under vacuum at 40°C until a constant weight was achieved.

2.5 Synthesis of 2-benzylidene malononitrile derivatives (3a–l)

A reaction mixture comprising aldehyde ${\bf 1a-l}$ (1 mmol) and malononitrile 2 (1 mmol) in the presence of basil– ${\rm Fe_3O_4}$ nanoparticles (3 mmol%) as a heterogeneous catalyst was subjected to monowave irradiation at 120 watts for 3 min in 5 mL ethanol, as shown in Scheme 2. The reaction progress was monitored by TLC using a solvent system of ethyl acetate:n-hexane (1:3). Upon completion, the basil– ${\rm Fe_3O_4}$ nanoparticle catalyst was efficiently separated from the reaction mixture using an external magnet. The target products ${\bf 3a-l}$ were isolated by crystallization, achieved through the gradual addition of distilled water to the ethanolic solution. The structures of synthesized products ${\bf 3a-l}$ were confirmed by analyzing their melting points and performing FT-IR, ${}^1{\rm H}$ NMR, and ${}^{13}{\rm C}$ NMR spectroscopy.

2.6 Linearity test and determination of LOD and LOQ

A series of standard solutions with different concentrations (5, 10, 15, 20, and 25 mg·L $^{-1}$) were prepared to assess the linearity of the UV–Vis spectrophotometric method for quantitatively analyzing Congo red dye. The absorbance of each solution was measured at the maximum absorption wavelength ($\lambda_{\rm max}$) of Congo red dye using a UV–Vis spectrophotometer. A calibration curve was created by plotting

Scheme 2: Synthesis of 2-benzylidene malononitrile derivatives 3a-1 utilizing basil– Fe_3O_4 nanocatalyst under microwave radiations at 120 W.

absorbance against concentration, and linear regression analysis was conducted to find the correlation coefficient (R^2) . The method was deemed linear if the R^2 value was ≥ 0.99 , indicating a strong relationship between absorbance and concentration within the tested range. This validation confirms the reliability and accuracy of the spectrophotometric method for determining Congo red dye concentration in degradation studies.

The limit of detection (LOD) and limit of quantification (LOQ) for analyzing Congo red dye using UV–Vis spectrophotometry were established based on the standard deviation of the blank and the slope of the calibration curve. The LOD indicates the smallest concentration that can be detected, though it may not be quantifiable, while the LOQ signifies the minimum concentration that can be accurately and precisely quantified.

To determine these values, a series of blank measurements were conducted, and the standard deviation (σ) of these readings was calculated. The calibration curve was created by plotting the absorbance against concentration, with the slope (S) derived from the linear regression equation. The formulas used for calculating LOD and LOQ are as follows:

$$LOD = \frac{3.3 \times \sigma}{S}$$

$$LOQ = \frac{10 \times \sigma}{S}$$

where σ refers to the standard deviation of blank absorbance measurements, and S refers to the slope of the calibration curve.

The resulting LOD and LOQ values indicate the sensitivity of the method, confirming its effectiveness for detecting and quantifying Congo red dye in studies of photocatalytic degradation.

2.7 Photochemical degradation of Congo red dye

For the photocatalytic degradation experiment, a $100~\text{mg}\cdot\text{L}^{-1}$ solution of Congo red dye was prepared in deionized water. The 5% of basil–Fe₃O₄ nanoadsorbent was then added to the solution. In the control study, no basil–Fe₃O₄ nanocatalyst was introduced into the dye solution. Instead, a 10~W UV lamp emitting light at a wavelength of 498 nm was submerged in the dye solution. To prevent interference from external light, the entire beaker was placed inside a light-blocking box. Before initiating the photocatalytic process, the mixture was stirred for 30~min to achieve equilibrium.

The degradation process was monitored by sampling the dye solution at regular intervals (1, 2, 3, 4, 5, and 6 h), and the concentration of Congo red dye was determined using UV–Vis spectroscopy.

During the degradation process, samples were taken at regular intervals over the course of an hour, then centrifuged, and their absorbance was measured using UV–Vis spectroscopy at 498 nm for the Congo red dye. The photocatalytic activity was evaluated by observing changes in absorbance in comparison to a control sample. The catalyst was magnetically recovered, cleaned, and reused through several cycles to assess its recyclability and stability. The degradation efficiency was calculated as a percentage uptake, reflecting the ratio of adsorbed dye to the initial amount of dye.

3 Result and discussion

3.1 Characterization of basil-Fe₃O₄ nanoparticles

3.1.1 FT-IR characterization

The FT-IR spectrum of basil–Fe $_3$ O $_4$ nanoparticles, presented in Figure 1, revealed key characteristic peaks. It can be observed that two prominent peaks between 551.02 and 773.01 cm $^{-1}$ resemble the Fe–O stretching mode within the crystalline structure of Fe $_3$ O $_4$, confirming the successful formation of the magnetic nanoparticles. Furthermore, bands identified at 1,621 and 3,235 cm $^{-1}$ were associated with the

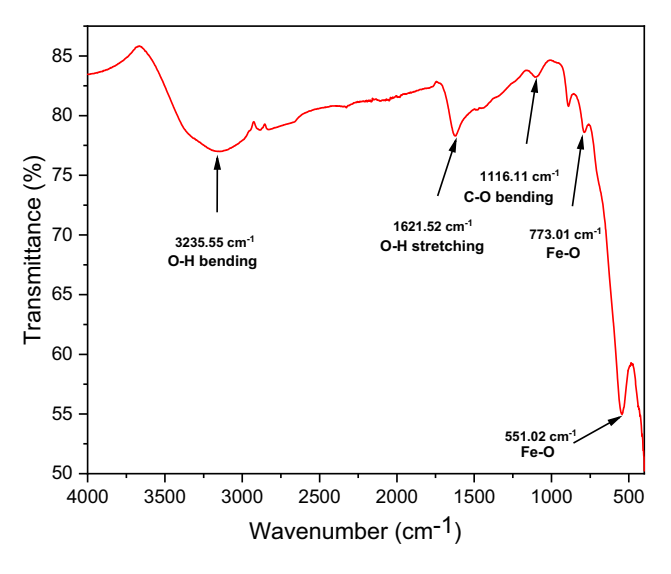


Figure 1: The FT-IR spectrum of basil-Fe₃O₄ nanoparticles.

bending and stretching modes of hydroxyl (–OH) groups, respectively. These peaks suggested the presence of surface hydroxyl groups, likely originating from both the Fe_3O_4 core and the phytochemical components of the basil extract.

Additionally, a significant peak observed at 1,116 cm⁻¹ corresponded to the C–O bond vibrations, indicating the presence of phytochemicals from basil leaf extract. The phytochemicals played a dual role, acting as reducing agents during nanoparticle synthesis and as capping agents, stabilizing the nanoparticles.

3.1.2 Optical and bandgap analysis

The analysis of the optical properties and band gap of basil–Fe $_3$ O $_4$ nanoparticles offers valuable insights into their potential uses, as shown in Figure 2. The UV–visible absorption spectrum showed a strong peak at 263 nm, indicating effective photon absorption in the UV range. The band gap energy, calculated from the Tauc plot, was determined to be 3.87 eV, which is significantly higher than that of conventional Fe $_3$ O $_4$ (approximately 2.8 eV) [35]. This notable increase in the band gap suggests a strong impact from the green synthesis method, likely due to surface modifications and interactions with bioactive compounds from the basil extract. The wider band gap improves the material's photostability and charge carrier separation, making it an excellent candidate for UV-driven photocatalytic applications, optoelectronic devices, and environmental cleanup.

Furthermore, the presence of plant-derived functional groups on the nanoparticle surface is crucial for adsorption and catalytic activity. Phytochemicals such as flavonoids, polyphenols, and terpenoids from basil extract can serve as natural stabilizers and surface modifiers, introducing functional groups like hydroxyl (-OH) and carboxyl (-COOH). These groups enhance surface interactions with pollutants, boosting adsorption capacity by facilitating hydrogen bonding, electrostatic interactions, and π - π stacking. The increased surface functionality also supports the effective degradation of organic contaminants by enhancing the active sites for photocatalysis. Therefore, the presence of phytochemicals not only affects nanoparticle synthesis but also significantly enhances their adsorptive and photocatalytic efficiency, making basil-Fe₃O₄ nanoparticles highly suitable for environmental remediation applications.

3.1.3 Scanning electron microscope characterization

The SEM images revealed nanoparticles with a cubic morphology and irregular shapes, as shown in Figure 3(a)–(c).

6 — Tamal Das et al. DE GRUYTER

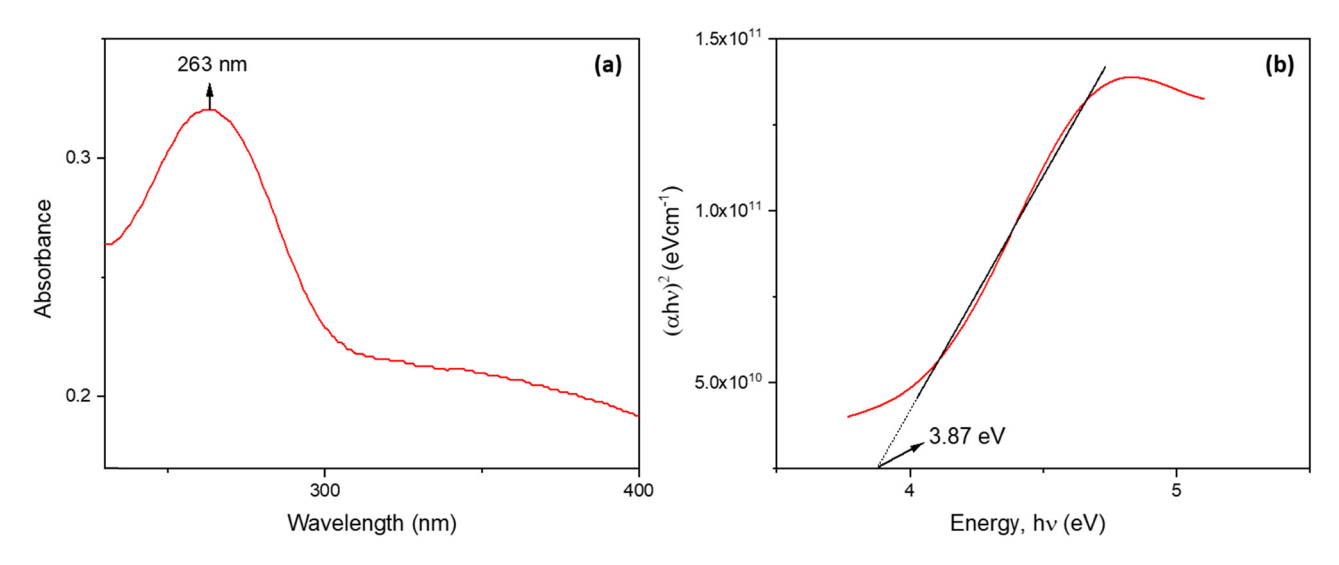


Figure 2: (a) UV-Vis adsorption spectrum and (b) Tauc plot of basil-Fe₃O₄ nanoparticles.

This morphology suggested variability in the growth patterns during the synthesis process, which is influenced by the interaction of the phytochemicals of the basil extract with the Fe_3O_4 crystal structure.

The images also demonstrated a significant degree of particle agglomeration, forming form-like clusters. This tendency to agglomerate was attributed to the magnetic property of the Fe_3O_4 nanoparticles, which promote magnetic dipole–dipole interaction, leading to particle clustering. Such behavior is consistent with the observation from previous studies on the magnetically active nanoparticle, where the magnetic force overcomes repulsive interactions, causing aggregation [36]. Moreover, the rough surface and non-uniform distribution of nanoparticles in the SEM images indicated the possible presence of phytochemicals capping agents from the basil extract. These agents not only influenced the particle morphology but also provided stabilization during particle formation.

The EDS analysis of basil– Fe_3O_4 nanoparticles (Figure 4) confirmed their elemental composition, revealing clear peaks for Fe and O that align with the formation of Fe_3O_4 . The

elemental composition (Fe: 37.53 ± 2.82 atom%, O: 64.47 ± 3.66 atom%) was in close agreement with theoretical values, indicating structural consistency. Sharp peaks observed between 0–1 and 6–8 keV validated the crystalline nature of the nanocatalyst. Furthermore, trace elements from basil-derived phytochemicals could enhance their catalytic and adsorption properties, highlighting their potential for sustainable applications.

3.1.4 XRD characterization

The XRD analysis of the magnetic nanoparticles derived from basil leaf extract is referred to as powder X-ray diffraction (PXRD), given that the sample is in powdered form. PXRD is utilized to assess the crystalline structure, phase composition, crystallite size, and purity of the synthesized nanoparticles. The peaks corresponding exclusively to Fe_3O_4 were observed, which are common by-products in the chemical co-precipitation process. This purity highlighted the efficiency of the synthesis method and the

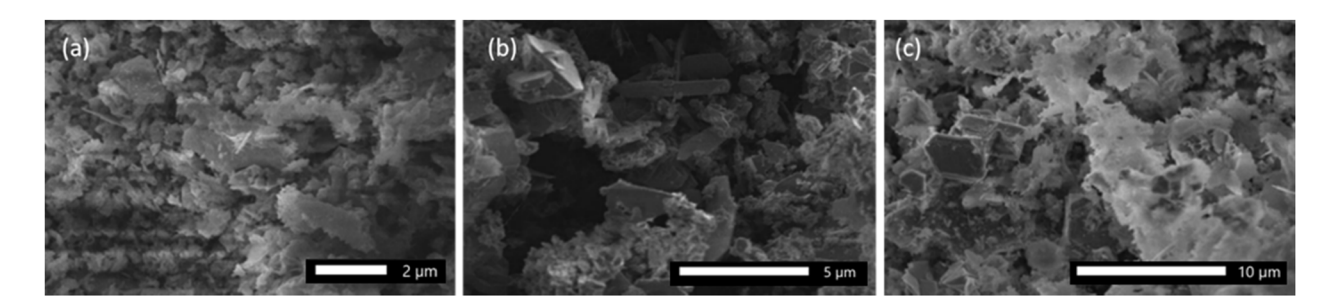


Figure 3: (a-c) SEM images of basil-Fe₃O₄ nanoparticles.

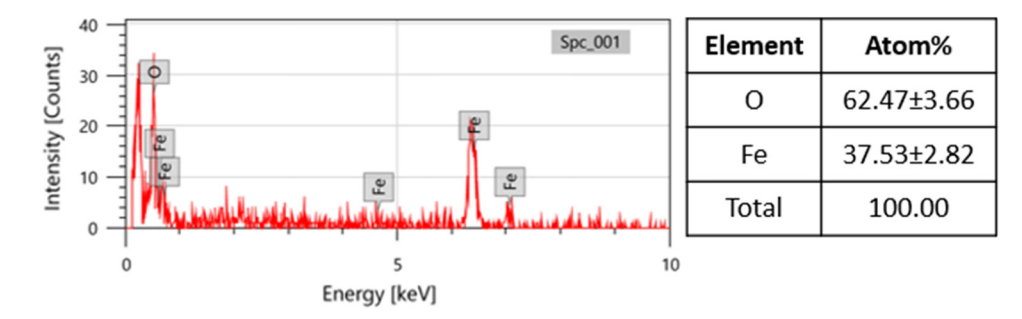


Figure 4: EDS-SEM analysis of basil-Fe₃O₄ nanoparticles.

stabilizing effect of the basil extract during the hydrothermal process.

The XRD spectra of basil– Fe_3O_4 nanoparticles, with the diffraction peaks indexed to Fe_3O_4 nanoparticles according to JCPDS No. 39-1346, is shown in Figure 5. The synthesized nanoparticles exhibited distinct diffraction peaks at $2\theta=31.213, 34.532, 36.942, 43.743, 53.712, 57.442$, and 64.531, which were indexed to the (220), (311), (222), (400), (422), (511), and (440) planes, respectively. The absence of additional peaks confirmed the high crystallinity and purity of the synthesized nanoparticles with no impurities or secondary phases. Using the Scherrer equation, the average crystallite size was calculated at 11 nm. The successful synthesis of pure nanoparticles with well-defined crystallinity and uniform size distribution demonstrated the effectiveness of the green synthesis approach utilizing basil extract.

In this study, we calculated the crystallite size of the synthesized nanoparticles using the Scherrer equation, a common method for estimating the size of coherently diffracting domains from XRD patterns. This approach offers

190 (331) 180 170 160 150 140 130 JCPDS 39-1346 120 110 40 50 60 70 2 Theta

Figure 5: XRD spectra of basil– Fe_3O_4 nanoparticles indexed to Fe_3O_4 nanoparticles (JCPDS No. 39-1346).

important insights into the structural properties of nanomaterials by linking the broadening of diffraction peaks to the crystallite size. The Scherrer equation is expressed as

$$D = \frac{K\lambda}{\beta\cos\theta}$$

where D represents the crystallite size, K is the shape factor (usually taken as 0.9), λ denotes the wavelength of the X-ray used (for instance, 0.15406 nm for Cu K α radiation), β is the full width at half maximum (FWHM) of the diffraction peak (measured in radians), and θ is the Bragg angle.

3.1.5 Zero-point charge analysis

Congo red has a pKa value of about 4.1, which is important for its adsorption and degradation behavior. The zero-point charge (pH $_{\rm zpc}$) of basil–Fe $_2$ O $_3$ nanoparticles was found to be 7.12, as illustrated in Figure 6, based on zeta potential measurements taken at different pH levels. The pH $_{\rm zpc}$ is a key factor in adsorption and photocatalysis

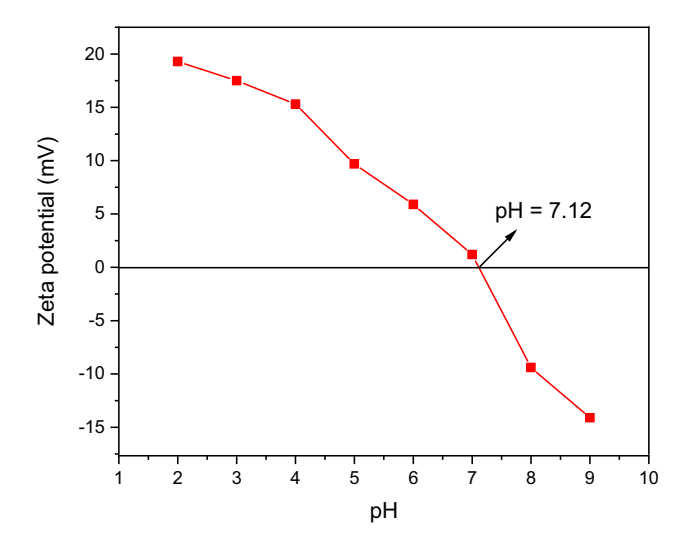


Figure 6: Zero-point charge of basil-Fe₃O₄ nanoparticles.

because it determines how the surface charge of the nanocatalyst behaves in various pH environments. At a pH of 7.12, the surface charge is neutral, meaning that there is no electrostatic attraction between the adsorbent and charged species in the solution. When the pH exceeds 7.12, the surface of the basil– Fe_2O_3 nanoparticles becomes negatively charged, which enhances the adsorption of cationic pollutants through electrostatic interactions. On the contrary, at pH levels below 7.12, the surface is positively charged, aiding the adsorption of anionic species like Congo red dye through electrostatic attraction.

Since Congo red has a pK_a of 4.1, it stays in its anionic form at pH values above this level, which improves its adsorption onto positively charged surfaces at lower pH values. The basil leaf extract affects Fe_2O_3 nanoparticles by introducing phytochemicals such as polyphenols, flavonoids, and terpenoids, which serve as capping agents, altering surface charge, dispersion, and catalytic activity. Functional groups (–OH, –COOH) enhance the interaction with pollutants, boosting adsorption and degradation efficiency across different pH conditions, making the nanocatalyst effective for wastewater treatment.

3.1.6 Vibrating-sample magnetometer characterization

The magnetic properties of basil–Fe₃O₄ nanoparticles were evaluated, as shown in Figure 7, and demonstrated their superparamagnetic nature. This was revealed by the magnetization curve intersecting the origin, indicating that the nanoparticles showed zero magnetization when an external magnetic field was absent. The saturation

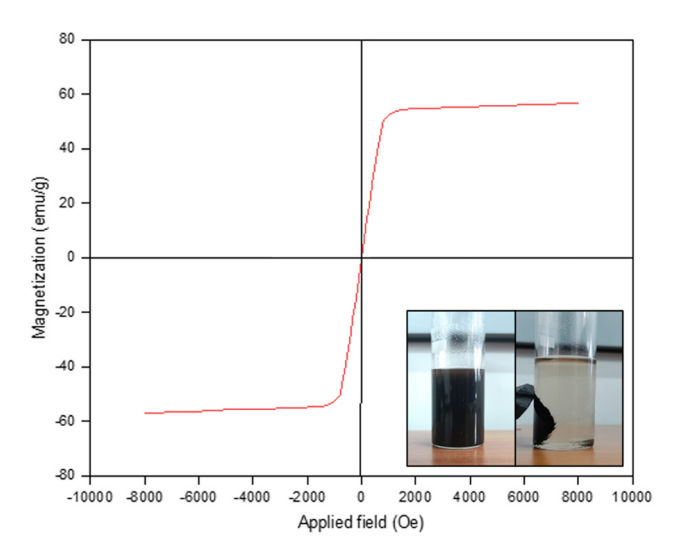


Figure 7: VSM curve of basil– Fe_3O_4 nanoparticles at 300 K obtained by a vibrating sample magnetometer.

magnetization measured at 300 K is 58.25 emu g^{-1} , a value comparable to those reported in previous studies on the saturation magnetization of Fe_3O_4 nanoparticles. While slightly lower than the bulk saturation magnetization of magnetite, this reduction was due to the nanoscale dimensions (9–12 nm) of the particles and the presence of organic capping agents from the basil extract.

3.2 Optimizing conditions for the synthesis of compound 3a

Following the characterization of the basil–Fe $_3O_4$ nanocatalyst, its efficacy was evaluated for the synthesis of 2-benzylidene malononitrile derivative **3a**. To optimize the reaction conditions for maximum yield and high purity, a comprehensive investigation was conducted, including the assessment of catalyst loading, choice of solvents, power of monowave reactor, and screening with various aldehyde substrates.

A model reaction was chosen using benzaldehyde **1a** (1 mmol) and malononitrile **2** (1 mmol) in the presence of 5 mmol% basil— Fe_3O_4 nanoparticles as a catalyst. The reaction was performed in ethanol (5 mL) under monowave irradiation at 100 W for 10 min. This approach provided an efficient and rapid method for synthesizing the target compound, leveraging the catalytic properties of the basil— Fe_3O_4 nanoparticles and the advantages of monowave-assisted synthesis.

3.2.1 Influence of catalyst loading on the synthesis of compound 3a

The model reaction was initially performed both in the absence and presence of the basil– Fe_3O_4 nanocatalyst, using varying catalyst loadings. In the absence of the catalyst, the synthesis of the target product, $\bf 3a$, yielded significantly low amounts. However, the introduction of the basil– Fe_3O_4 nanocatalyst notably enhanced the yield of $\bf 3a$, demonstrating its excellent catalytic efficiency in facilitating the reaction.

It was noted that increasing the catalyst loading led to an improvement in yield and a reduction in the reaction time. Nevertheless, beyond the optimal catalyst loading of 3 mmol% (entry 3, Table 1), no significant improvement in product yield was recorded. Moreover, the reaction time increased slightly. This behavior was attributed to the saturation of the active sites on the catalyst at higher loadings, which led to mass transfer limitations and a consequent reduction in catalytic efficiency.

Table 1: Impact of the basil-Fe₃O₄ nanocatalyst loading on synthesis of compound 3a

Entry Catalyst loading (mmol%)		Yield* (%)	
1	1	90	
2	2	91	
3	3	95	
4	4	89	
5	5	76	

^{*}Yield refers to the total production output of all crops.

3.2.2 Influence of solvent for the synthesis of compound 3a

Subsequent experiments investigated the influence of various solvents on the model reaction, including water, ethanol, a water/ethanol (1:1) mixture, toluene, glycerol, DMF, and acetonitrile, as well as solvent-free conditions. Among these, ethanol was found to provide excellent yields of 3a within a shorter reaction time (entry 3, Table 2). Based on these observations, the optimized conditions for further experiments were determined to be a catalyst loading of 3 mmol% basil-Fe₃O₄ nanocatalyst in ethanol under monowave irradiation at 100 W for 10 min.

3.2.3 Optimization of microwave reactor power for the synthesis of compound 3a

In the subsequent step, the optimized conditions were utilized to determine the optimal power setting for synthesizing various 2-benzylidene malononitrile derivatives using the basil–Fe₃O₄ nanocatalyst. As shown in Table 3, higher power levels resulted in increased yields over time. However, increasing the power beyond 120 W resulted in a decrease in yield, as the elevated temperatures caused by higher power led to product decomposition. As a result, 120 W (entry 4,

Table 2: Influence of solvents on the synthesis of compound 3a using basil-Fe₃O₄ nanocatalyst

Entry	Solvent	Yield* (%)
1	No solvent	_
2	Toluene	56
3	Water	70
4	Ethanol	95
5	Water/ethanol (1:1)	81
6	Glycerol	67
7	DMF	82
8	Acetonitrile	89

^{*}Yield refers to the total production output of all crops.

Table 3: Influence of power on percentage yield of compound 3a using basil-Fe₃O₄ nanocatalyst

Entry	Watt	Time (min)	Yield* (%)
1	90	10	90
2	100	8	92
3	110	5	93
4	120	3	98
5	130	3	96
6	140	3	92

^{*}Yield refers to the total production output of all crops.

Table 3) was determined to be the optimal condition for achieving excellent conversion into 2-benzylidene malononitrile under previously established standard conditions.

The synthesis of 2-benzylidene malononitrile derivatives was optimized using 3 mmol% basil-Fe₃O₄ nanoparticles as a catalyst in 5 mL of ethanol, applying microwave irradiation at 120 watts for 3 min. This method allowed for a quick and efficient response, resulting in high-purity crystalline products. The application of microwave irradiation notably shortened the reaction time while improving product selectivity and yield, showcasing the effectiveness of the basil-Fe₃O₄ nanocatalyst in facilitating greener and more sustainable synthetic processes.

3.2.4 Screening of aldehyde substrates for the synthesis of 2-benzylidene malononitrile derivatives (3a-l)

Under optimal conditions, a variety of 2-benzylidene malononitrile derivatives 3a-I were synthesized using different aromatic aldehydes to examine the versatility of the reaction with basil–Fe₃O₄ nanocatalyst. The reaction exhibited excellent performance with a variety of aromatic and heterocyclic aldehydes 1a-I, as summarized in Table 4. Notably, the desired products 3a-I were obtained in high to excellent yields within a short reaction time. Aromatic aldehydes featuring carboxylic rings with electron-withdrawing groups 1a-g (entries 1-7, Table 4) were investigated, along with aldehydes containing electron-donating groups 1h-k and the electron-rich heterocyclic aldehyde 11. Under the optimized conditions, these substrates effectively produced the corresponding 2-benzylidene malononitrile derivatives 3h-I (entries 8-12, Table 4).

3.3 Characterization of 2-benzylidene malononitrile 3a using basil-Fe₃O₄ nanocatalyst

The structure of compound 3a was confirmed using various spectroscopic methodologies, including FT-IR, ¹H and 10 — Tamal Das et al. DE GRUYTER

Table 4: Synthesis of 2-benzylidene malononitrile derivatives 3a-l using basil-Fe₃O₄ nanocatalyst under MW irradiations at 120 W

Entry	R	2-Benzylidene malononitrile derivatives (3a–l)	Time (min)	Yield (%)	MP (°C)	Lit. MP (°C)	Reference
1	C ₆ H ₅ (1a)	H N (3a)	3	98	87-88	83-85	[9]
2	3-NO ₂ C ₆ H ₄ (1b)	H N	2	97	113–114	107–109	[25]
3	4-NO ₂ C ₆ H ₄ (1c)	NO ₂ (3b)	2	96	158-159	160–161	[9]
4	2-CIC ₆ H ₄ (1d)	H	3	97	95–96	92-94	[20]
5	4-CIC ₆ H ₄ (1e)	(3d) H N (3e)	3	95	165–166	163–164	[25]
6	3-BrC ₆ H ₄ (1f)	H	3	96	148–149	150–152	[16]
7	4-BrC ₆ H ₄ (1g)	Br (3f)	3	93	151–153	153–155	[9]
8	4-MeOC ₆ H ₄ (1h)	H ₃ CO (3h)	2	97	112–114	114–116	[25]
9	4-CH ₃ C ₆ H ₄ (1i)	H	3	95	138–140	134–136	[16]
10	C ₆ H₅CH=CH (1j)	H ₃ C (3i)	3	98	115–118	111–113	[24]
11	4-Me ₂ NC ₆ H ₄ (1k)	H ₃ C _{-N} H	2	94	67-69	63-66	[16]
12	2-Furyl (1I)	он ₃ (3k)	3	98	180–182	182–183	[24]

^{*}Yield refers to the total production output of all crops.

 13 C NMR. In the FT-IR spectrum, stretching peaks at 3,032.91 cm $^{-1}$ indicated the presence of the sp 2 hybridized C–H bond, while a peak at 2,222.63 cm $^{-1}$ corresponded to C=N stretching. In 1 H NMR spectra (500 MHz, CDCl $_{3}$), the formation of a highly pure final product is confirmed. A

singlet at δ 7.77 ppm was assigned to the C–H bond, and singlets from δ 7.53 to 7.93 ppm were assigned to aromatic protons.

In 13 C NMR (125 MHz, CDCl $_3$), the most downfield peak at δ 159.1 ppm corresponded to the C-1 carbon. Additional

peaks at δ 133.7 (C-1'), 129.9 (C-2' and C-6'), 129.7 (C-3' and C-5'), and 128.6 ppm (C-4') were observed in the aromatic region. The peaks for the two C \equiv N groups and C-2 carbon appeared at 112.7, 111.6, and 81.7 ppm, respectively. The melting point of the synthesized compound **3a** (87–88°C) was consistent with its literature values (83–85°C), further confirming the successful synthesis of the final product.

malononitrile **(3a)** derivative. The basil– Fe_3O_4 nanocatalyst imparted magnetic properties to the Fe_3O_4 nanocatalyst, enabling easy recovery and reuse via a magnet. After each experimental cycle, the basil– Fe_3O_4 nanocatalyst was retrieved, washed twice with distilled water and acetone, and dried before being used for the subsequent cycles. Table 5 presents the outcomes of the catalyst recycling over four consecutive runs.

3.4 Investigation of reusability of magnetic basil–Fe₃O₄ nanocatalyst for synthesis of 2-benzylidene malononitrile derivatives

The investigation of this study aimed to evaluate the recyclability of the nanoparticles, which was tested using an optimized reaction scheme to synthesize the 2-benzylidene

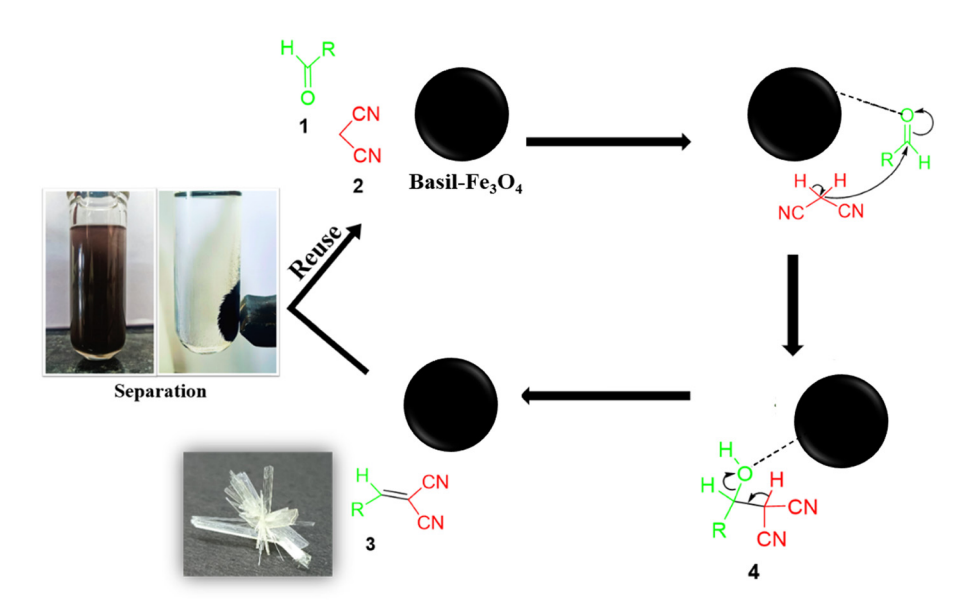
Table 5: Reusability of basil $-Fe_3O_4$ nanocatalyst for synthesis of 2-benzylidene malononitrile $\bf 3a$

Cycle	Yield* (%)
1	98
2	96
3	95
4	92
5	91

^{*}Reusability of nanocatalyst for 2-benzylidene malononitrile derivatives synthesis.

3.5 Plausible mechanism for the synthesis of 2-benzylidene malononitrile derivatives

According to the previous literature, a plausible mechanism is proposed for the synthesis of 2-benzylidene malononitrile 3a via a two-component reaction between substituted aldehyde 1 and malononitrile 2, as depicted in Scheme 3 [4]. The proposed mechanism suggests that the basil-Fe₃O₄ nanocatalyst activated the substituted benzaldehyde 1 by increasing the electrophilicity of its carbonyl carbon. This activation is hypothesized to occur through the formation of H bonds between the nanocatalyst and the O atom of the carbonyl group of substituted aldehydes. Concurrently, hydrogen bonding is proposed between the nanocatalyst and the acidic hydrogen of malononitrile. These interactions facilitate the Knoevenagel condensation, producing an intermediate compound 4, which subsequently undergoes rearrangement to form the targeted compound 3a.



Scheme 3: Mechanism synthesis of 2-benzylidene malononitrile derivatives 3a-I using basil-Fe₃O₄ nanoparticles.

Tamal Das et al. DE GRUYTER

Table 6: Comparison of basil-Fe₃O₄ nanoadsorbent with other reported nanoadsorbents for the synthesis of 2-benzylidene malononitrile derivatives

Nanoadsorbent	Reaction conditions	Yield (%)	Reusability	Reference
Fe₃O₄–cysteamine hydrochloride nanoparticles	Solvent-free, 60°C, ultrasonic bath, 6 h	96	Yes	[37]
Fe₃O₄@SiO₂@SO₃H nanoparticles	Room temperature, ethanol, 6-8 h	95	Yes	[38]
Ag ₂ CO ₃ -containing magnetic nanocomposite	Solvent-free, 60°C, ultrasonic bath, 6–8 h	96	Yes	[39]
Proline–Cu complex based Fe₃O₄ nanoparticles	Room temperature, water, 8-10 h	91	Yes	[40]
Basil–Fe ₃ O ₄ nanoadsorbent	Monowave irradiation at 120 watts, 3 min	98	Yes	This work

3.6 Comparison of synthesis of 2-benzylidene malononitrile derivatives with other reported nanoadsorbents

The comparative analysis of different nanoadsorbents for synthesizing 2-benzylidene malononitrile derivatives reveals that the basil– Fe_3O_4 nanoadsorbent developed in this study outperforms the others, as discussed in Table 6. Our catalyst achieves an impressive 98% yield in just 3 min using monowave irradiation at 120 W. In comparison, other catalysts like Fe_3O_4 —cysteamine hydrochloride nanoparticles and Ag_2CO_3 -containing magnetic nanocomposites take significantly longer, requiring 6–8 h to reach a 96% yield under solvent-free conditions at 60°C with ultrasonic assistance. Likewise, Fe_3O_4 @Si O_2 @SO $_3$ H nanoparticles and proline—Cu complex-based Fe_3O_4 nanoparticles need 6–10 h to obtain yields between 91% and 95% at room temperature in ethanol or water.

The impressive effectiveness of the basil–Fe $_3$ O $_4$ nanoadsorbent in producing 2-benzylidene malononitrile derivatives can be linked to several important factors. First, using monowave irradiation at 120 W greatly speeds up the reaction kinetics, cutting the reaction time down to just 3 min. Second, the combined effect of the bioactive compounds found in basil extract and the Fe $_3$ O $_4$ nanoparticles boosts the catalytic activity, resulting in higher yields. Furthermore, the eco-friendly and sustainable synthesis method that employs basil extract not only offers a green alternative but also adds functional groups that may aid the catalytic process. Together, these elements

Table 7: Measurements of the absorbance of Congo red dye solution

Sample Concentration (mg· L^{-1})		Absorbance
Blank	0	0.000
Standard 1	5	0.042
Standard 2	10	0.056
Standard 3	15	0.060
Standard 4	20	0.075
Standard 5	25	0.086

lead to the quick and effective synthesis achieved with the basil– Fe_3O_4 nanoadsorbent.

3.7 Linearity test and determination of LOD and LOQ

3.7.1 Linearity test

The linearity of the UV–Vis spectrophotometric method used for quantifying Congo red dye was evaluated by measuring the absorbance of standard solutions with concentrations between 5 and $25~{\rm mg\,L^{-1}}$, as shown in Table 7. A calibration curve was created by plotting absorbance against concentration, and linear regression analysis was conducted to find the correlation coefficient (R^2). The resulting R^2 value of 0.99099 indicates a strong linear relationship between absorbance and concentration, confirming that Beer–Lambert's law is applicable within the studied range.

This observed linearity suggests that the UV–Vis spectrophotometric method developed is appropriate for quantitatively determining Congo red dye in aqueous solutions, as shown in Figure 8. The slight deviations in absorbance

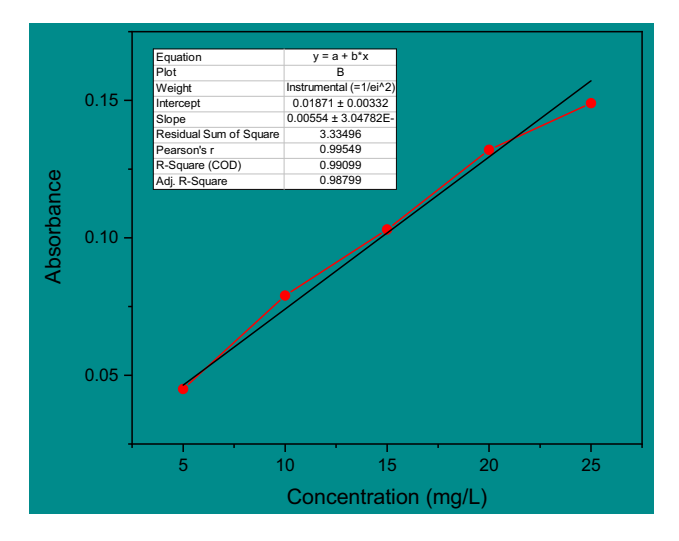


Figure 8: Congo red dye standard solution calibration curve.

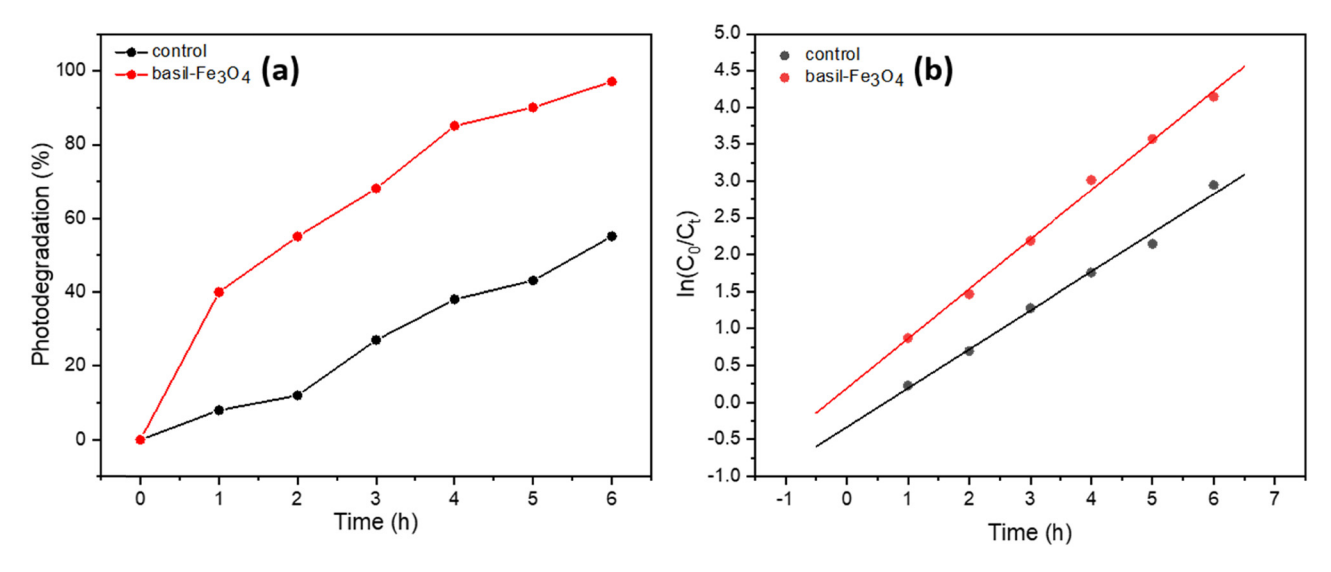


Figure 9: (a) Photocatalytic degradation of Congo red dye with UV–Vis irradiation, (b) first-order kinetic plot for photocatalytic degradation of Congo red dye by basil–Fe₃O₄ nanoadsorbent.

values at higher concentrations may be due to minor instrumental variations or interactions within the dye solution. Nevertheless, the overall high R^2 value (>0.99) supports the method's reliability and accuracy for subsequent photocatalytic degradation studies. This validation ensures that the spectrophotometric method can effectively track the degradation efficiency of the catalyst by analyzing the decrease in Congo red dye concentration over time.

The LOD and LOQ are crucial parameters that assess the sensitivity and reliability of an analytical method. The LOD indicates the lowest concentration of an analyte that can be detected, though it may not be quantifiable, while the LOQ represents the minimum concentration that can be accurately and precisely quantified, adhering to the required accuracy standards. In the UV–Vis spectrophotometric analysis of Congo red dye, the LOD and LOQ were determined using the standard deviation of blank measurements along with the slope of the calibration curve, which is 0.00554. The calculated values were LOD = $32.8 \, \text{mg} \cdot \text{L}^{-1}$ and LOQ = $99.16 \, \text{mg} \cdot \text{L}^{-1}$, demonstrating the method's effectiveness in detecting and quantifying Congo red dye within the specified concentration range. The relatively high LOQ indicates that this method is

particularly suitable for monitoring Congo red dye at moderate to high concentrations, making it relevant for studies on photocatalytic degradation. These findings confirm that the UV–Vis spectrophotometric method offers a robust response in detecting Congo red dye, ensuring its applicability in environmental and analytical contexts.

3.8 Photocatalytic Congo red dye degradation

The photocatalytic activity of the basil– Fe_3O_4 nanocatalyst was assessed by comparing the degradation efficiency of Congo red dye with and without the catalyst when exposed to UV light. As shown in Figure 9, after 6 h of UV exposure, only 55% degradation was observed without the catalyst, while the use of basil– Fe_3O_4 resulted in a remarkable 97% degradation. This highlights the catalyst's impressive efficiency, as even a small quantity (5%) was able to effectively degrade a substantial amount of dye under low UV irradiation, suggesting its potential for large-scale applications.

The photocatalytic performance of the basil– Fe_3O_4 nanocatalyst was significantly better than that of the

Table 8: Kinetic data of photocatalytic degradation of Congo red dye by basil-Fe₃O₄ nanoadsorbent

Photocatalytic activity	Photodegradation of Congo red (%)*	Kinetic constant, k	Regression coefficient (R^2)
Control	55	0.0022	0.9915
Basil–Fe ₃ O ₄	97	0.0097	0.9962

^{*}The amount of basil-Fe₃O₄ nanoadsorbent was 5%.

control, as indicated in Table 8. In the absence of the catalyst, only 55% of the Congo red dye was degraded over a period of 6 h, with a kinetic constant (k) of 0.0022 min⁻¹ and an R^2 value of 0.9915. In comparison, the use of basil–Fe₃O₄ led to a remarkable 97% degradation, with higher k values of 0.0097 min⁻¹ and an improved R^2 of 0.9962, which confirms enhanced reaction efficiency and first-order kinetics. These findings underscore the outstanding photocatalytic activity of basil–Fe₃O₄, demonstrating its effectiveness in degrading dyes when exposed to UV light.

These findings underscore the efficiency of basil-Fe₃O₄ nanocatalyst in accelerating the degradation process compared to the control. Its high degradation rate and superior kinetic performance establish it as a promising candidate for environmental remediation applications. The excellent photocatalytic performance of the basil-Fe₃O₄ nanocatalyst can be linked to its large surface area, effective charge separation, and strong magnetic properties, all of which improve its stability and reusability. The Fe₃O₄ nanoparticles help generate electron-hole pairs when exposed to UV light, which in turn promotes the creation of reactive species that effectively degrade dyes. Moreover, the bioactive compounds found in basil extract may enhance the catalytic activity. The increased kinetic constant and improved regression coefficient further validate the enhanced reaction efficiency compared to the control, positioning basil-Fe₃O₄ as a promising catalyst for wastewater treatment.

3.9 Comparison of photocatalytic degradation of Congo red dye with other reported nanoadsorbents

The comparison of photocatalytic degradation efficiencies of various nanoadsorbents, including $Fe_3O_4/ZnO/LC$ (54.8%), $SnO_2-Fe_3O_4$ (50.76%), and $Fe_3O_4@TiO_2$ (96%), highlights the impressive performance of the basil– Fe_3O_4 nanocatalyst (97%) developed in our work, as depicted in Table 9.

While the Fe₃O₄-based composites with TiO₂ showed good performance due to TiO₂'s known photocatalytic

Table 9: Comparison of basil– Fe_3O_4 nanoadsorbent with reported nanoadsorbents for photocatalytic degradation of Congo red dye

Nanoadsorbent	Photocatalytic degradation of Congo red dye (%)	Reference	
Fe ₃ O ₄ /ZnO/LC	54.8	[31]	
SnO ₂ -Fe ₃ O ₄	50.76	[32]	
Fe ₃ O ₄ @TiO ₂	96	[33]	
Basil-Fe ₃ O ₄	97	This work	

capabilities, the addition of basil leaves to Fe_3O_4 in our study enhanced the photocatalytic activity beyond traditional composites, achieving nearly complete degradation of Congo red dye. The lower efficiencies of $Fe_3O_4/ZnO/LC$ and $SnO_2-Fe_3O_4$ (both below 60%) can be attributed to limitations in charge separation, dye interaction, or insufficient surface area, which are addressed in our work through the bio-inspired modification. This enhancement demonstrates that integrating bio-based materials, such as basil, with magnetic nanocatalysts can significantly improve photocatalytic performance, offering a more sustainable and efficient approach for dye degradation in wastewater treatment.

3.10 Plausible mechanism for dye degradation using basil-Fe₃O₄ nanoadsorbent

According to previous studies on potential mechanisms, the degradation of dye using basil-Fe₃O₄ nanoadsorbent is mainly influenced by the photocatalytic activity of the Fe₃O₄ nanoparticles [41]. The dye degradation mechanism using basil-Fe₃O₄ nanoadsorbent is primarily driven by the photocatalytic activity of the Fe₃O₄ nanoparticles, enhanced by the biofunctional groups derived from basil leaves [41]. Under UV irradiation, the Fe₃O₄ nanoparticles serve as effective electron donors, which, when activated, generate ROS such as hydroxyl radicals (OH) and superoxide anions (O_2^{-}) . These ROS play a crucial role in breaking down organic pollutants like Congo red dye. The basil leaf-derived functional groups, particularly phenolic compounds, facilitate the adsorption of the dye onto the nanoadsorbent surface, promoting better interaction between the dye molecules and the active sites on the catalyst. Additionally, the magnetic properties of Fe₃O₄ enable easy recovery and reuse of the nanocatalyst, further enhancing its sustainability and efficiency in continuous degradation processes. The combination of efficient charge separation, ROS generation, and dye adsorption due to the basil leaf's bioactive components results in a highly effective photocatalytic system for the degradation of organic dyes in wastewater treatment.

4 Conclusion

In this study, we presented an eco-friendly and recyclable method for synthesizing 2-benzylidene malononitrile derivatives using a highly efficient and reusable basil—Fe₃O₄

nanocatalyst under microwave irradiation. This approach achieved impressive product yields (up to 98%) with excellent purity in a remarkably short reaction time of just 3 min at 120 W. The basil-Fe₃O₄ nanocatalyst showed outstanding catalytic performance, allowing for easy magnetic recovery and reusability, maintaining a 95% yield in the second cycle and 90% even after five cycles. The process was cost-effective, labor-efficient, and environmentally friendly, operating under mild conditions with minimal waste generation. Moreover, the basil-Fe₃O₄ nanocatalyst exhibited exceptional photocatalytic efficiency, achieving 97% degradation of Congo red dye, which significantly outperformed conventional catalysts. Optical analysis indicated a band gap energy of 3.87 eV, contributing to its superior photocatalytic performance. Additionally, calculations for LOD (32.8 mg·L⁻¹) and LOQ (99.16 mg·L⁻¹) confirmed the method's sensitivity and reliability in detecting Congo red dye. The catalyst's ability to effectively degrade pollutants with minimal UV exposure (even at 5%) makes it highly suitable for large-scale wastewater treatment applications. This study emphasizes the dual functionality of basil-Fe₃O₄ nanocomposites in both organic synthesis and environmental remediation, highlighting their potential as a sustainable and versatile solution for green chemistry and wastewater treatment. These findings suggest promising implications for greener, more efficient chemical processes across various industrial applications.

Acknowledgments: The authors thank the Researchers Supporting Project Number (RSPD2025R729), King Saud University, Riyadh, Saudi Arabia. PKB and HH sincerely acknowledge financial support from the National Institute of General Medical Sciences (GM103440) of the National Institutes of Health, USA. PKB sincerely acknowledges the MUREP Partnership Learning Annual Notification (MPLAN) Prize sponsored by NASA. HH sincerely acknowledges the Faculty Opportunity Award (FOA) that is administered by the Office of Sponsored Programs (OSP) at UNLV. PKB also sincerely acknowledges the Knowledge Fund that is administered by the Nevada Governor's Office of Economic Development (GOED) and the University of Nevada Las Vegas (UNLV). The authors also thank Chandigarh University, Gharuan, Punjab, India for providing all the basic facilities to carry out this research.

Funding information: The authors would like to thank the Researchers Supporting Project Number (RSPD2025R729), King Saud University, Riyadh, Saudi Arabia.

Author contributions: Tamal Das: writing – original draft; Harvinder Singh Sohal: methodology and supervision; Fohad Mabood Husain and Pradip K. Bhowmik: investigation; Manvinder Kaur and Navneet Kaur: data collection, writing - review and editing; Haesook Han: data analysis and review.

Conflict of interest: The author states no conflicts of interest.

Data availability statement: All data generated or analyzed during this study are included in this published article (and its Supplementary Information files).

References

- Somwanshi PB, Somvanshi SB, Kharat SB. Nanocatalyst: A brief review on synthesis to applications. J Phys Conf Ser. 2020;1644(1):1-30. doi: 10.1088/1742-6596/1644/1/012046.
- Dalessandro EV, Collin HP, Valle MS, Pliego IR, Mechanism and free energy profile of base-catalyzed Knoevenagel condensation reaction. RSC Adv. 2016;6(63):57803-10. doi: 10.1039/c6ra10393f.
- Orchard KL, Shaffer MSP, Williams CK. Organometallic route to [3] surface-modified ZnO nanoparticles suitable for in situ nanocomposite synthesis: Bound carboxylate stoichiometry controls particle size or surface coverage. Chem Mater. 2012;24(13):2443-8. doi: 10.1021/cm300058d.
- Zhuo C, Xian D, Jian-wei W, Hui X. An efficient and recyclable ionic liquid-supported proline catalyzed knoevenagel condensation. ISRN Org Chem. 2011;2011:1-5. doi: 10.5402/2011/676789.
- [5] Wang CW, Gu B, Liu QQ, Pang YF, Xiao R, Wang SQ. Combined use of vancomycin-modified Aq-coated magnetic nanoparticles and secondary enhanced nanoparticles for rapid surface-enhanced Raman scattering detection of bacteria. Int J Nanomed. 2018;13:1159-78. doi: 10.2147/IJN.S150336.
- Hong RY, Li JH, Cao X, Zhang SZ, Di GQ, Li HZ, et al. On the Fe₃O₄/ Mn_{1-x}Zn_xFe₂O₄ core/shell magnetic nanoparticles. J Alloys Compd. 2009;480(2):947-53. doi: 10.1016/j.jallcom.2009.02.098.
- Irfan M, Dogan N, Bingolbali A, Aliew F. Synthesis and characterization of NiFe₂O₄ magnetic nanoparticles with different coating materials for magnetic particle imaging (MPI). J Magn Magn Mater. 2021;537(1):1-20. doi: 10.1016/j.jmmm.2021.168150.
- Kalantari F, Rezayati S, Manafi Moghadam M, Ramazani A. A novel Cu (II) nanoparticles anchored on cyanuric chloride-attached magnetic nanocatalyst: A highly stable, recyclable and efficient nanocatalyst for the synthesis of chromene derivatives. Inorg Chem Commun. 2024;164(1):112371. doi: 10.1016/j.inoche.2024.112371.
- [9] Hosain ANA, El Nemr A, El Sikaily A, Mahmoud ME, Amira MF. Surface modifications of nanochitosan coated magnetic nanoparticles and their applications in Pb(II), Cu(II) and Cd(II) removal. | Environ Chem Eng. 2020;8(5):1-23. doi: 10.1016/j.jece. 2020.104316.
- Lu Y, Lu X, Mayers BT, Herricks T, Xia Y. Synthesis and characterization of magnetic Co nanoparticles: A comparison study of three different capping surfactants. J Solid State Chem. 2008;181(7):1530-8. doi: 10.1016/j.jssc.2008.02.016.
- Haniffa MA, Munawar K, Chee CY, Pramanik S, Halilu A, Illias HA, et al. Cellulose supported magnetic nanohybrids: Synthesis, physicomagnetic properties and biomedical applications-A review. Carbohydrate Polymers. 2021;267:1-22. Elsevier Ltd, doi: 10.1016/j. carbpol.2021.118136.

- [12] Rho WY, Kim HM, Kyeong S, Kang YL, Kim DH, Kang H, et al. Facile synthesis of monodispersed silica-coated magnetic nanoparticles. J Ind Eng Chem. 2014;20(5):2646–9. doi: 10.1016/j.jiec.2013.12.014.
- [13] Doan L. Surface modifications of superparamagnetic iron oxide nanoparticles with polyvinyl alcohol and activated charcoal as methylene blue adsorbents. Magnetochemistry. 2023;9(9):1–20. doi: 10.3390/magnetochemistry9090211.
- [14] Prathna TC, Sitompul DN, Sharma SK, Kennedy M. Synthesis, characterization and performance of iron oxide/alumina-based nanoadsorbents for simultaneous arsenic and fluoride removal. Desalin Water Treat. 2018;104:121–34. doi: 10.5004/dwt.2018.21960.
- [15] Ahamad T, Naushad M, Al-Shahrani T, Al-hokbany N, Alshehri SM. Preparation of chitosan based magnetic nanocomposite for tetracycline adsorption: Kinetic and thermodynamic studies. Int J Biol Macromol. 2020;147:258–67. doi: 10.1016/j.ijbiomac.2020.01.025.
- [16] Kumar ASK, Jiang SJ. Synthesis of magnetically separable and recyclable magnetic nanoparticles decorated with β-cyclodextrin functionalized graphene oxide an excellent adsorption of As(V)/ (III). J Mol Liq. 2017;237:387–401. doi: 10.1016/j.molliq.2017.04.093.
- [17] Appaturi JN, Ratti R, Phoon BL, Batagarawa SM, Din IU, Selvaraj M, et al. A review of the recent progress on heterogeneous catalysts for Knoevenagel condensation. Dalt Trans. 2021;50(13):4445–69. doi: 10.1039/d1dt00456e.
- [18] Rezayati S, Morsali A. Functionalization of magnetic UiO-66-NH2 with a Chiral Cu(l-proline)2 complex as a hybrid asymmetric catalyst for CO₂ conversion into cyclic carbonates. Inorg Chem. Apr 2024;63(13):6051–66. doi: 10.1021/acs.inorgchem.4c00376.
- [19] Stoimenov PK, Klinger RL, Marchin GL, Klabunde KJ. Metal oxide nanoparticles as bactericidal agents. Langmuir. 2002;18(17):6679–86. doi: 10.1021/la0202374.
- [20] Ruban SM, Ramadass K, Singh G, Talapaneni SN, Kamalakar G, Gadipelly CR, et al. Organocatalysis with carbon nitrides. Sci Technol Adv Mater. 2023;24(1):1–20. doi: 10.1080/14686996.2023.2188879.
- [21] Zhuang B, Yang Y, Huang K, Yin J. Plasmon-enhanced NIR-II photoluminescence of rare-earth oxide nanoprobes for highsensitivity optical temperature sensing. Opt Lett. 2024;49(22):6489–92. doi: 10.1364/OL.540944.
- [22] Bhuiyan MMH, Hossain M, Ashraful Alam M, Mahmud MM. Microwave assisted Knoevenagel condensation: Synthesis and antimicrobial activities of some arylidene-malononitriles. Chem J. 2012;2(1):30–6.
- [23] Carvalho HL, de Amorim AL, Araújo IF, Marino BLB, Jimenez DEQ, Ferreira RMA, et al. A simple and efficient protocol for the knoevenagel reaction of benzylidenemalononitriles and the evaluation of the larvicidal activity on aedes Aegypti. Rev Virtual Quim. 2018;10(2):362–74. doi: 10.21577/1984-6835.20180028.
- [24] Zhang X, He X, Zhao S. Preparation of a novel $Fe_3O_4@SiO_2@propyl@DBU \ magnetic \ core-shell \ nanocatalyst for Knoevenagel reaction in aqueous medium. Green Chem Lett Rev. 2021;14(1):83–96. doi: 10.1080/17518253.2020.1862312.$
- [25] Abbasi M, Harifi-Mood AR, Lotfi Nosood Y. Reaction kinetics investigation of Malononitrile with substituted benzaldehydes in aqueous solutions of ethaline as deep eutectic solvent. Int J Chem Kinet. 2020;52(8):513–9. doi: 10.1002/kin.21366.
- [26] Ajay PSS, Pandya U, Chaudhari MP, Sharma VS, George A, Shiyal GN. Application of Fe₃O₄@MCC Nanoparticles as a heterogeneous catalyst for sustainable multicomponent synthesis of 2,3'-Biindoles. ChemCatChem. 2024;1(2):1–25. doi: 10.1002/cctc. 202401308
- [27] Osman PS, Zhang AI, Farghali Y, Rashwan M, Eltaweil AK, Abd El-Monaem AS, et al. Synthesis of green nanoparticles for

- energy, biomedical, environmental, agricultural, and food applications: A review. Environ Chem Lett. 2024;22(2):841–87. doi: 10.1007/s10311-023-01682-3, Springer International Publishing.
- [28] Fatima S, Shahid H, Zafar S, Arooj I, Ijaz S, Elahi A. Ocimum basilicum seed-mediated green synthesis of silver nanoparticles: characterization and evaluation of biological properties. Discover Nano. 2024;19(1):172. doi: 10.1186/s11671-024-04130-5.
- [29] Yazdanpanah G, Heidari MR, Amirmahani N, Nasiri A. Heterogeneous Sono-Fenton like catalytic degradation of metronidazole by Fe₃O₄@HZSM-5 magnetite nanocomposite. Heliyon. 2023;9(6):e16461. doi: 10.1016/j.heliyon.2023.e16461.
- [30] Golestani N, Nasiri A, Hashemi M. CoFe₂O₄ @MC/AC as an efficient and recyclable magnetic nanohybrid adsorbent for the metronidazole removal from simulated wastewater: bioassays and whole effluent toxicity. Desalin Water Treat. 2022;280:312–29. doi: 10.5004/dwt.2022.29118.
- [31] Zhao A, Tang Q, Chen Y, Qiu C, Huang X. Tetracycline and congo red from aqueous solution. Molecules. 2023;28:6499–6514. doi: 10.3390/molecules28186499.
- [32] Said M, Rizki WT, Asri WR, Desnelli D, Rachmat A, Hariani PL. SnO₂–Fe₃O₄ nanocomposites for the photodegradation of the Congo red dye. Heliyon. 2022;8(4):1–18. doi: 10.1016/j.heliyon.2022.e09204.
- [33] Arora P, Fermah A, Rajput JK, Singh H, Badhan J. Efficient solar light-driven degradation of Congo red with novel Cu-loaded Fe₃O₄@TiO₂ nanoparticles. Environ Sci Pollut Res. 2017;24(24):19546–60. doi: 10.1007/s11356-017-9571-7.
- [34] Gogoi A, Baithy M, Navgire M, Gogoi N, Borgohain C, Kamal Senapati K, et al. Development of highly efficient heterogeneous Fe₃O₄-biochar nanocomposite as fenton-like catalysts for degradation of fast green. Chem Sel. 2023;8(41):1–22. doi: 10.1002/slrt 202302553
- [35] Delice S, Isik M, Gasanly NM. Temperature-dependent tuning of band gap of Fe₃O₄ nanoparticles for optoelectronic applications. Chem Phys Lett. 2024;840:141139. doi: 10.1016/j.cplett.2024.141139.
- [36] Wardani RK, Dahlan K, Wahyudi ST, Sukaryo SG. Synthesis and characterization of nanoparticle magnetite for biomedical application. AIP Conference Proceedings. vol. 2194; 2019. p. 4–9, doi: 10.1063/1.5139869.
- [37] Dehghani P, Elhamifar D, Kargar S. Amine functionalized magnetic resorcinol formaldehyde as a green and reusable nanocatalyst for the Knoevenagel condensation. Sci Rep. 2025;15(1):2873. doi: 10.1038/s41598-025-85921-3.
- [38] Shekhanavar R, Khatavi SY, Kamanna K. Green method synthesis of magnetic nanoparticles and its functionalized MNPs for knoevenagel condensation reaction. Curr Organocatal. 2024;11(4):330–43. doi: 10.2174/0122133372292087240228082859.
- [39] Fatemeh Karimkhah MS, Elhamifar D. Ag₂CO₃ containing magnetic nanocomposite as a powerful and recoverable catalyst for Knoevenagel condensation. Sci Rep. 2021;11(1):18736–49. doi: 10.1038/s41598-021-98287-z.
- [40] Kalantari F, Rezayati S, Ramazani A, Aghahosseini H, Ślepokura K, Lis T. Proline-Cu complex based 1,3,5-triazine coated on Fe₃O₄ magnetic nanoparticles: a nanocatalyst for the knoevenagel condensation of aldehyde with malononitrile. ACS Appl Nano Mater. Feb 2022;5(2):1783–97. doi: 10.1021/acsanm.1c03169.
- [41] Maruthupandy M, Muneeswaran T, Vennila T, Anand M, Cho W-S, Quero F. Development of chitosan decorated Fe₃O₄ nanospheres for potential enhancement of photocatalytic degradation of Congo red dye molecules. Spectrochim Acta, Part A. 2022;267:120511. doi: 10.1016/j.saa.2021.120511.